



Published in final edited form as:

Ann Eye Sci. 2020 September ; 5: . doi:10.21037/aes-20-81.

Retinal imaging in inherited retinal diseases

Michalis Georgiou^{1,2}, Kaoru Fujinami^{1,2,3}, Michel Michaelides^{1,2}

¹UCL Institute of Ophthalmology, University College London, London, UK

²Moorfields Eye Hospital NHS Foundation Trust, London, UK

³Laboratory of Visual Physiology, Division of Vision Research, National Institute of Sensory Organs, National Hospital Organization Tokyo Medical Center, Tokyo, Japan

Abstract

Inherited retinal diseases (IRD) are a leading cause of blindness in the working age population. The advances in ocular genetics, retinal imaging and molecular biology, have conspired to create the ideal environment for establishing treatments for IRD, with the first approved gene therapy and the commencement of multiple therapy trials. The scope of this review is to familiarize clinicians and scientists with the current landscape of retinal imaging in IRD. Herein we present in a comprehensive and concise manner the imaging findings of: (I) macular dystrophies (MD) [Stargardt disease (*ABCA4*), X-linked retinoschisis (*RS1*), Best disease (*BEST1*), pattern dystrophy (*PRPH2*), Sorsby fundus dystrophy (*TIMP3*), and autosomal dominant drusen (*EFEMP1*)], (II) cone and cone-rod dystrophies (*GUCA1A*, *PRPH2*, *ABCA4* and *RPGR*), (III) cone dysfunction syndromes [achromatopsia (*CNGA3*, *CNGB3*, *PDE6C*, *PDE6H*, *GNAT2*, *ATF6*), blue-cone monochromatism (*OPN1LW/OPN1MW* array), oligocone trichromacy, bradyopsia (*RGS9/R9AP*) and Bornholm eye disease (*OPN1LW/OPN1MW*), (IV) Leber congenital amaurosis (*GUCY2D*, *CEP290*, *CRB1*, *RDH12*, *RPE65*, *TULP1*, *AIPL1* and *NMNAT1*), (V) rod-cone dystrophies [retinitis pigmentosa, enhanced S-Cone syndrome (*NR2E3*), Bietti crystalline corneoretinal dystrophy (*CYP4V2*)], (VI) rod dysfunction syndromes (congenital stationary night blindness, fundus albipunctatus (*RDH5*), Oguchi disease (*SAG*, *GRK1*), and (VII) chorioretinal dystrophies [choroideremia (*CHM*), gyrate atrophy (*OAT*)].

Open Access Statement: This is an Open Access article distributed in accordance with the Creative Commons Attribution-NonCommercial-NoDerivs 4.0 International License (CC BY-NC-ND 4.0), which permits the non-commercial replication and distribution of the article with the strict proviso that no changes or edits are made and the original work is properly cited (including links to both the formal publication through the relevant DOI and the license). See: <https://creativecommons.org/licenses/by-nc-nd/4.0/>.

Correspondence to: Professor Michel Michaelides. UCL Institute of Ophthalmology, 11-43 Bath Street, London EC1V 9EL, UK. michel.michaelides@ucl.ac.uk.

Contributions: (I) Conception and design: All authors; (II) Administrative support: None; (III) Provision of study materials or patients: All authors; (IV) Collection and assembly of data: All authors; (V) Data analysis and interpretation: All authors; (VI) Manuscript writing: All authors; (VII) Final approval of manuscript: All authors.

Provenance and Peer Review: This article was commissioned by the Guest Editor (R Theodore Smith) for the series “Retinal Imaging and Diagnostics” published in *Annals of Eye Science*. The article was sent for external peer review organized by the Guest Editor and the editorial office.

Conflicts of Interest: The authors have completed the ICMJE uniform disclosure form (available at <http://dx.doi.org/10.21037/aes-20-81>). The series “Retinal Imaging and Diagnostics” was commissioned by the editorial office without any funding or sponsorship. The authors have no other conflicts of interest to declare.

Ethical Statement: The authors are accountable for all aspects of the work in ensuring that questions related to the accuracy or integrity of any part of the work are appropriately investigated and resolved.

Keywords

Retinal imaging; inherited retinal disease; retinitis pigmentosa; macular dystrophy; leber congenital amaurosis

Introduction

The inherited retinal diseases (IRD) have heterogeneous clinical presentation, which can result in diagnostic challenge. Diagnosis commonly involved multimodal retinal imaging, as well as psychophysical and electrophysiological evaluation. They constitute the leading cause of legal blindness in England and Wales amongst working-age adults, and the second commonest in childhood (1), having a great impact on the individuals and families affected (2), and they are subject to a range of interventions and research avenues (3). Here, we categorise IRD on the basis of the primarily affected retinal cell-type and disease natural history (stationary or progressive). We prioritised the selected conditions based on: (I) their prevalence, (II) ongoing trial(s) of novel therapeutics, and (III) distinctive imaging findings.

Macular dystrophies (MD)

MD are a group of IRD characterised by bilateral, relatively symmetrical macular abnormalities that significantly impair central visual function (4). Below we present the imaging findings of the commonest subtypes (5), including Stargardt disease (STGD), Best disease (BD), X-linked retinoschisis (XLR5), Sorsby fundus dystrophy (SFD), pattern dystrophy (PD), and autosomal dominant drusen (ADD).

Stargardt disease

STGD (*ABCA4*, OMIM 601691) is the most common MD. The most common presentation is a widespread deposition of lipofuscin (bisretinoids) in the retinal pigment epithelium (RPE), leading to the classical fundus appearance of retinal flecks. The spectrum of disease is highly variable, ranging from generalised cone and rod system involvement (COD/CORD *ABCA4* disease is presented in the next section) to isolated macular disease (Figure 1A) (6–11). Fundus fluorescein angiography (FFA) demonstrates a dark choroidal phase due to masking from lipofuscin deposition in the RPE; but has been superseded by optical coherence tomography (OCT) and fundus autofluorescence (FAF). A characteristic pattern of areas of increased and decreased signal on FAF imaging is seen in STGD. FAF imaging may serve as a monitoring tool, and decreased autofluorescence area measurements can be used as a structural outcome for interventional clinical trials (12,13). The peripheral fundus FAF findings and the classification of the posterior pole appearance can be achieved with Ultra-wide field FAF (UWF-FAF) (14–17).

OCT sensitively quantifies RPE atrophy and the severity and extent of outer retinal loss (photoreceptor loss). Moreover, it can identify asymptomatic childhood-onset STGD, by demonstrating hyperreflectivity at the base of the foveal outer nuclear layer (6). The anatomical level of the retinal flecks can be demonstrated and can be correlated with visual function (9,10,18–22). The earliest structural changes of the disease are juxtafoveal and

appear to spare the foveola (6). Photoreceptor loss is likely to precede RPE degeneration; both of which contribute to choriocapillaris loss (23,24). *In vivo* cellular imaging using adaptive optics (AO), proved reduced cone densities and increased photoreceptor spacing (25,26). The cones can be reliably counted, and tracked over time (27).

BD

BD (*BEST1*, OMIM 607854) is the second most common MD and is an autosomal dominant condition, due to disease-causing variants in *BEST1* (28). Early stage (Stage 1) disease is characterised by a normal fundus or minimal RPE changes (pre-vitelliform). The classical appearance of BD is the single, bilateral symmetrical egg-yolk-like (vitelliform) lesion at the fovea (Stage 2). Over time, this lesion can start to undergo resorption, progressing to a ‘pseudohypopyon’ (Stage 3). The subretinal yellow material gravitates inferiorly within the lesion. Stage 1 and 2 are associated with normal visual acuity (VA), and patients can be identified during a family survey or co-incidentally. VA reduction is observed from stage 3 onwards. Further breakdown of subretinal material can result in a ‘vitelliruptive stage’ (Stage 4). End-stage disease (Stage 5) is characterised by either sub-RPE fibrosis (29), atrophy, or choroidal neovascularisation (CNV). Despite the classification of the fundus appearance into stages, there is rarely predictable progression from one to the other.

The subretinal vitelliform lesion presents with a high signal on FAF imaging and it is best visualized with OCT (Figure 1B) (30). A common finding is subretinal fluid (SRF) which waxes and wanes over time. Inherited causes of vitelliform lesion can be distinguished from non-inherited acquired disorders due to the increased signal on FAF. The fibrosis that can occur in advanced BD has been described as resembling a “circus tent” due to its exaggerated height and unusual height-to-base ratio (31). OCTA has suggested this fibrosis to have a neovascular origin (32). Fibrotic lesions appear hypoautofluorescent on FAF. OCTA is particularly useful in identifying CNV in vitelliform disorders including BD, where FFA can be very challenging to interpret (4).

XLRS

XLRS (*RS1*, OMIM 312700) is the most common form of juvenile-onset retinal degeneration in males (4). The hallmark feature of XLRS is the “spoke-wheel” folds of the macula (macular schisis) (Figure 1C). Peripheral retinal changes are observed in approximately 50% of males, including, schisis (with inner or outer retinal holes), pigmentary disturbance, white spiculations, metallic sheen, neovascularisation and vitreous veils. An increased risk of rhegmatogenous retinal detachment (RD), or vitreous haemorrhage (VH) has been reported for patients with peripheral retinoschisis (33). Bullous XLRS can be congenital or develop soon after birth, and it can be complicated later in life by RD, which may be rhegmatogenous, tractional or a Coats-like exudative detachment (34). The development of macular atrophy may lead to slow VA loss in older adults.

The identification of macular schisis can be challenging on clinical examination, making multimodal imaging invaluable. Splitting of the inner and outer retinal layers can be readily identified with OCT, and a spoke-wheel appearance of concentric areas of high- and low-signal intensity is observed with FAF imaging (Figure 1C). Rarely macular OCT can be

normal/near normal, and peripheral changes are then the only clue to the clinical diagnosis. Ultra-wide field imaging with FFA and OCTA can be helpful identifying less common vascular abnormalities such as vascular sheathing and neovascularization (35). Increased and irregular cone spacing within the foveal schisis is reported with AO imaging. However, the presence of preserved wave-guiding cones at the fovea and macular regions may indicate a good potential for successful rescue with intervention (23,36).

Sorsby fundus dystrophy

SFD (*TIMP3*, OMIM 188826) is a rare ADD-associated MD. FAF imaging may identify a broad ill-defined increase in signal in the peripheral macula in early disease, with subretinal drusenoid deposits - reticular pseudodrusen, that spare the central fovea, clearly depicted on infra-red imaging (Figure 1D). OCT can identify drusen-like deposits and delineate Bruch membrane thickening; and is valuable in the diagnosis of CNV. Early CNV changes can be captured with OCTA, without the need for FFA (37).

PD

PD (*PRPH2*, OMIM 179605) is characterized by variable distributions of pigment deposition at the level of the RPE. The deposits in PD are typically hyperautofluorescent on FAF, and may result in a characteristic speckled pattern (38). As these changes are at the level of RPE, subretinal hyper-reflective material is seen on OCT (Figure 1E).

ADD

ADD (*EFEMP1*, OMIM 601548) is an autosomal dominant condition characterised by drusen-like deposits at the macula, which may be in a radiating (*Malattia leventinese*) or honeycomb-like appearance [Doyme honeycomb retinal dystrophy (MIM126600)]. The drusen-like deposits in ADD are hyperautofluorescent on FAF, in contrast to drusen in AMD which are variable on FAF (39,40). Drusen-like deposits are seen as hyper-reflective thickening of the RPE-Bruch membrane complex (41), with disrupted photoreceptor integrity on OCT (Figure 1F) (42). CNV in ADD can be diagnosed with OCTA (43).

Cone and cone-rod dystrophies

Progressive COD/CORD are characterised by cone photoreceptor degeneration, which may be followed by subsequent rod photoreceptor loss. These disorders typically present with progressive loss of central vision, colour vision disturbance and photophobia (11,44). We discuss their retinal imaging, focusing on five of the most common genotypes: *GUCA1A*, *GUCY2D*, *ABCA4*, *PRPH2* and *RPGR*.

Autosomal dominant *GUCA1A*-associated COD/CORD

GUCA1A COD/CORD (OMIM 600364) has variable funduscopy findings, ranging from mild RPE disturbance to extensive macular atrophy (Figure 2A). FAF is useful in investigating macular abnormalities, although both areas of hypoautofluorescence and hyperautofluorescence have correlated with retinal atrophy; an increased signal at the fovea may be seen in early disease (45–47). Cellular variability between patients harbouring the same variant is identified with AOSLO (48).

Autosomal dominant *GUCY2D*-associated COD/CORD

GUCY2D (OMIM 600179) variants can cause both COD, CORD, and Leber congenital amaurosis (LCA) (49,50). *GUCY2D*-associated COD/CORD is AD disease, in contrast to LCA which is recessive (51). Fundoscopy findings are varied, ranging from mild RPE changes to extensive macular atrophy, observed in older individuals (52,53). FAF imaging usually shows central hypoautofluorescence and a surrounding ring of hyperautofluorescence (Figure 2B) (53). A variable degree of EZ disruption over the fovea can be observed, as well as macular thinning (54).

Autosomal dominant *PRPH2*-associated CORD

PRPH2 COD/CORD (OMIM 179605) fundoscopic appearance ranges from a bull's-eye maculopathy to macular atrophy. A characteristic speckled macular appearance on FAF is demonstrated in most of the patients (Figure 2C) (55). AOSLO imaging in p.(Arg172Trp)-associated CORD revealed increased cone spacing throughout the macula with corresponding loss of outer retinal structures on OCT (56). However, intrafamilial analysis of p.(Arg172Gln)-associated disease has shown marked variability, similar to that seen in *GUCA1A*-associated CORD; whilst one family member had a completely normal photoreceptor mosaic, two others had variable parafoveal cone loss (57).

Autosomal recessive *ABCA4*-associated COD/CORD

ABCA4 COD/CORD (OMIM 601691), fundoscopy may initially reveal a normal fundus or mild retinal abnormalities (such as loss of foveal reflex), whereas peripheral degenerative changes occur in later disease (58). Diagnosis can therefore be delayed unless FAF or OCT imaging is undertaken (8). FAF findings include a bull's-eye maculopathy-like appearance with yellow-white retinal flecks and increasing macular atrophy over time (59,60); whilst OCT reveals loss of outer retinal architecture at the central macula (24). Longitudinal increase in abnormal AF regions correlates with both visual function decline and abnormal cone spacing on AOSLO (61). However, cone mosaic abnormalities are known to precede abnormal psychophysical testing and FAF (25).

X-Linked *RPGR*-associated COD/CORD

Most disease-causing variants in *RPGR* (OMIM 312610) result in retinitis pigmentosa (RP) (62), but those leading to COD/CORD are preferentially sequestered at the 3' end of the ORF15 region (63). FAF imaging often reveals parafoveal rings of increased signal in *RPGR*-associated COD/CORD (Figure 2D). Unlike RP, these increase in size with disease progression and are inversely related to ERG amplitude (64,65).

Cone dysfunction syndromes (CDS)

The CDS are stationary cone disorders, with congenital/early-infantile onset and give rise to purely cone dysfunction, whereas the aforementioned progressive cone dystrophies are of later-onset and usually also involve rod loss over time (66). CDS are rarer than COD/CORD, with only 10 genes implicated and only five distinct phenotypes described to date; achromatopsia (ACHM), blue-cone monochromatism (BCM), oligocone trichromacy (OT),

bradyopsia and Bornholm eye disease (BED). Retinal imaging of all these conditions will be described.

ACHM

ACHM is the most common CDS. Disease-causing variants have been reported in *CNGA3* (67,68) (OMIM600053), *CNGB3* (69) (OMIM605080), *GNAT2* (70,71) (OMIM139340), *ATF6* (72) (OMIM605537), *PDE6H* (73) (OMIM601190) and *PDE6C* (66) (OMIM600827). It presents either at birth or early infancy, with poor VA, pendular nystagmus, photophobia, and color vision loss along all three axes (74).

Four distinct FAF phenotypes have been reported: (I) normal appearance (Figure 3A), (II) central increased signal (Figure 3B), (III) reduced signal centrally (Figure 3C) (75), and (IV) central area of decreased signal (Figure 3D), with a surrounding ring of hyperautofluorescence (76). OCT imaging can be used to grade ACHM into five grades: (I) Continuous ellipsoid zone (EZ) (Figure 3E), (II) EZ disruption (Figure 3F), (III) EZ absence (Figure 3G), (IV) presence of a hyporeflective zone (Figure 3H), and (V) outer retinal atrophy with RPE loss (Figure 3I) (77). In *CNGA3* and *CNGB3* genotypes, all these grades have been observed (with approximately 50% cases being grade I to III); suggesting residual cones in a good proportion of patients. The presence of residual cones is critical for targeting by gene therapy intervention (78,79). In contrast for *PDE6C*-ACHM and *ATF6*-ACHM, no patients have been reported with grades I-II. *GNAT2*-ACHM typically presents with grade I (80). OCT findings support that the condition is predominantly stable in the vast majority of patients (81). In contrast, *PDE6C*-ACHM can be slowly progressive (76). Foveal hypoplasia, preservation of inner retinal layers over the fovea, is a common OCT finding in ACHM; being present in all subjects with *ATF6*-ACHM (Figure 3G) (76,82), in 60–70% of previously reported patients with *CNGA3*- and *CNGB3*-ACHM (Figure 3F) (77,78,83–85), and is not present in any reported subject with *GNAT2*- and *PDE6C*-ACHM.

ACHM is by far the most well-studied condition using AOSLO imaging (23). Marked variability in the cone mosaic has been observed across patients; with no significant difference between the two most common genotypes, *CNGA3* and *CNGB3* (77,83,86), and the rarer *GNAT2* genotype associated with the least disrupted photoreceptor mosaic (80,87,88). In a large cohort of *CNGB3*-ACHM, significantly decreased peak foveal cone densities and increased spacing has been reported (78). Similar findings were also reported for *CNGA3*-ACHM (n=38), also including a high degree of interocular symmetry, and vast intrafamilial variability (79). In *ATF6*- and *PDE6C*-associated ACHM, AOSLO studies identified few if any cellular residual structures (76,82).

Gene therapy trials for *CNGA3*- and *CNGB3*-associated ACHM are on-going.

Blue cone monochromatism

BCM is an X-linked condition characterized by defects of L- and M-wavelength-sensitive cone function (OMIM 300821, 300822, 300824), with a fundus examination revealing a myopic but otherwise normal retina (66,89). Presenting symptoms, OCT and FAF imaging can be similar to ACHM, with a variable degree of EZ disruption (Figure 3J) (90). In AOSLO imaging, cone mosaic disruption is highly variable and may be genotype specific

(23,91) The cone mosaic appears dark over the foveal centre with confocal AOSLO, with a sparse array of large bright spots, which are believed to be S-cones, surrounding it (91,92). Cone density is higher than that expected for the S-cone sub-mosaic, in keeping with remnant L-/M-cones (93–95). Overall, these AOSLO imaging studies have identified significant inter-subject variability (23). Despite female carriers being asymptomatic, confocal AOSLO has demonstrated variably reduced cone density, increased spacing, and disrupted organisation, with phenotypic variability likely relating to random X-chromosome inactivation (96).

BED

BED (OMIM 300821, 300822) is an X-linked CDS associated with dichromacy and myopia, decreased VA, RPE thinning, and visible choroidal vessels in the posterior pole (66,97). Retinal thinning can be observed on OCT (Figure 3K) (98). AOSLO imaging shows evidence that patients with BED have a significantly disrupted cone mosaic (23,98–100).

OT

The disease hallmark is the reduced amplitude of cone responses on ERG, with normal or near-normal color discrimination, and normal fundus appearance (66,101). On OCT imaging the outer segment length appears reduced, with decreased intensity of the EZ outside the fovea (102). The cone photoreceptor mosaic in OT has been investigated with an AO fundus camera, and in keeping with the original disease mechanism hypothesis, a decreased number ('oligocone') of otherwise normal appearing foveal cones (thereby permitting 'trichromacy') was observed (102).

RGS9/R9AP-associated retinopathy ('Bradyopsia')

RGS9/R9AP-associated retinopathy (OMIM 604067, 607814) presents from early childhood with delayed dark and light adaption (103), which can be a common feature also in OT (102), as well as other findings such as a normal fundus appearance, reduced VA, and normal color vision (104–107). OCT and FAF are usually normal (Figure 3L) (107). Unlike in OT, confocal AOSLO has revealed a normal cone photoreceptor mosaic in subjects with *RGS9/R9AP*-associated retinopathy (102,108). Cellular phenotyping is therefore able to differentiate between these two conditions with common clinical features—an intact photoreceptor mosaic in *RGS9/R9AP*-associated retinopathy, and disruption in OT (23).

LCA/EOSRD

LCA/EOSRD are both genetically and phenotypically heterogeneous, and characterised clinically by severe congenital/early infancy visual loss, nystagmus, amaurotic pupils and markedly reduced/absent full-field electroretinograms (109). The identified genes account for approximately 70–80%. *GUCY2D*, *CEP290*, *CRB1*, *RDH12* and *RPE65* are the most common and their imaging findings are presented below, together with *TULP1*, *AIP1* and *NMNAT1* due to distinctive findings are also presented.

GUCY2D - LCA/EOSRD

Patients with *GUCY2D*-LCA/EOSRD (OMIM 600179) often have relatively normal fundi, in contrast to most other LCA/EOSRD genotypes (51). There can be relatively preserved outer retinal structure on OCT in many patients (even lifelong, Figure 4A), although foveal cone outer segment abnormalities and foveal cone loss has been observed (51,110). FAF findings are variable; normal, central foveal hyperautofluorescence, and/or a perimacular ring of increased AF have been reported (Figure 4A) (51). A phase I/II gene therapy trial is on-going.

CEP290 - LCA/EOSRD

OCT studies of *CEP290*-LCA/EOSRD (OMIM 610142) have shown that despite profound cone dysfunction, the foveal architecture is structurally preserved until the fourth decade of life in some patients; although with abnormal inner and outer segments in contrast to the early loss of rod photoreceptors (110,111). FAF imaging reveals a perifoveal hyperautofluorescent ring in most patients (Figure 4B), and areas of decreased signal in older patients (pigmentary retinopathy) (111). Phase I/II and Phase III gene therapy trials are on-going.

CRB1 - LCA/EOSRD

CRB1-associated disease (OMIM 604210) has nummular pigmentation, maculopathy, relative preservation of para-arteriolar RPE, intraretinal cystoid spaces, with retinal thickening and loss of lamination on OCT (Figure 4C) (112). Not all findings are present in all patients. Altered retinal lamination with increased RNFL thickness; is a rather unique finding for *CRB1* compared to other LCA/EOSRD genotypes (113). *CRB1* variants can be associated with a range of phenotypes and corresponding retinal imaging findings; including RP (114), Coats-like vasculopathy, and maculopathy (115).

RDH12 - LCA/EOSRD

RDH12-associated disease (OMIM 608830), which gives rise to an EOSRD phenotype is characterised by early-dense intraretinal pigment migration and maculopathy (116). OCT reveals severe loss of structure often from 10 years of age (117). Macular atrophy is a universal finding on FAF (centrally decreased signal), and with disease progression, the area of atrophy extends peripherally in a variegated watercolour-like pattern (Figure 4D), which usually corresponds to the retinal vasculature (117). Recently the phenotypic spectrum of *RDH12* has been extended to include later onset and milder phenotypes (118).

RPE65 - LCA/EOSRD

RPE65-deficiency (OMIM 180069) is associated with reduced or absent AF on FAF imaging, suggesting low or absent levels of lipofuscin in the RPE (Figure 4E) (119,120). OCT studies have demonstrated relatively normal retinal thickness in some patients; with more commonly a central macular area of relatively preserved retina with a surrounding ring of thinning or more widespread retinal loss (Figure 4E) (120,121). There is an FDA- and EMA-approved gene therapy for *RPE65*-EOSRD.

TULP1, AIPL1 and NMNAT1 - LCA

TULP1 (OMIM 602280), *AIPL1* (OMIM 604323) and *NMNAT1* (OMIM 608700)-associated disease are characterised by early maculopathy. *NMNAT1* maculopathy typically is severe, early onset and extensive (Figure 4F), with pigment clumping (including nummular pigmentation), both visible on FAF and OCT (122). Similar to *RDH12*, the phenotypic spectrum of *NMNAT1* has been extended to later onset and a milder phenotype (123). In *AIPL1*-LCA no patient is identified in the literature with residual outer retinal structure beyond the age 4 (110,124). A gene therapy study is on-going for *AIPL1*-LCA.

Rod-cone dystrophies

Rod-cone dystrophies are a variable group of inherited retinal conditions, both in terms of phenotype and genotype (125), with a prevalence of 1/3,000–1/4,000 in the general population (126). Herein we present the imaging findings of RP, enhanced S-Cone syndrome (ESCS) and Bietti crystalline corneoretinal dystrophy (BCD).

RP

RP is characterized by nyctalopia and gradual constriction of the visual field, with eventual loss of central vision, progressing to legal blindness (127,128). RP can be inherited as an autosomal dominant, autosomal recessive (AR) or X linked trait. Due to the large number of genes involved (>100 genes) and the lack of distinct/specific genotype-phenotype correlations, an overview of retinal imaging will be presented for RP and not each specific genotype.

Areas of atrophied RPE/photoreceptor cell loss have decreased AF because of the lack of lipofuscin, and are observed to a greater extent in the mid-periphery (Figure 5A). Wide-field FAF can better evaluate the full extent of peripheral atrophy in RP. Increased AF is often observed in the form of a concentric ring around the macula (65), and represents areas of dysfunction/degenerating photoreceptors (129). The hyperautofluorescent ring demarcates the area of central viable retina from the surrounding atrophic retina, and thereby is observed to constrict over time (in contrast to *CORD*, where it is seen to expand) (65). The ring size and width follows an exponential decline, with faster loss of area earlier in the disease (65,130). X-linked forms of the disease are usually more severe, with early involvement of the fovea and more rapid decline of vision (Figure 5B) (131).

On OCT imaging the disruption of the photoreceptor layer (EZ) starts from the periphery (rod rich region) and gradually the functioning retina constricts to the fovea (Figure 5A), till it disappears, leading to blindness (Figure 5B). Both the width of the residual EZ, as well as the area of EZ on *en face* analysis, are established sensitive measure of RP progression (132,133). Several studies employing AOSLO have reported a decrease in cone density and/or increased cone spacing in patients with RP (23).

Sector RP is an uncommon restricted form of RP in which only one or two retinal quadrants display clinical pathological signs (Figure 5C), and as such is associated with a good prognosis (134). A phase I/II gene therapy trials is on-going for *PDE6B*, *MERTK*, *RPGR*, and *RLBPI*.

ESCS

ESCS (*NR2E3*, OMIM 268100) is a rare slowly progressive AR form of retinal degeneration, typically characterised by nummular pigment clumping at the level of the RPE, often most plentiful around the temporal vascular arcades (Figure 5D) (135). OCT studies may show a disturbed perimacular region (thought to be filled with S-cone photoreceptors instead of rods), with thick and bulging retina and abnormal laminar architecture (Figure 5D) (136). Other imaging findings include: torpedo-like changes, deep atrophic lesions with a small hyperpigmented rim, helicoid subretinal fibrosis, circumferential fibrotic scars in the posterior pole with a spared centre, large fibrotic scars around the optic nerve head, and yellow-white dots in areas of relatively normal-appearing retina (137,138).

BCD

BCD (*CYP4V2*, OMIM 608614) is an AR disease, with similar clinical symptoms to RP, associated with progressive RPE-choriocapillaris complex atrophy and retinal crystals (Figure 5E), which can disappear with disease progression, resulting in greater RPE disruption (139,140). FAF shows sharply demarcated areas of RPE loss that coincide with abrupt edges of outer retinal atrophy on OCT; with the crystals generally situated on or in, the RPE/Bruch's complex (139).

ROD Dysfunction syndromes

Rod Dysfunction syndromes are a genetically diverse group of non-progressive primary dysfunctions of the rod system, most commonly causing congenital stationary night blindness (CSNB) - with [Fundus Albipunctatus (FA) and Oguchi Disease] or without abnormal fundi (complete and incomplete CSNB) (141).

Complete and Incomplete Congenital Stationary Night Blindness (cCSNB/iCSNB)

In contrast to FA and Oguchi disease, which are described below, cCSNB/iCSNB have no distinctive fundus appearance with normal or myopic fundi (142). Electrophysiological findings are the key to differentiate cCSNB and iCSNB; complete dysfunction of on-pathway and incomplete dysfunction of both on- and off-pathways (143). cCSNB/iCSNB have a heterogeneous genetic background including AD, AR and X-linked, with variable VA and night blindness (141). Aland Eye Disease is a form of X-linked incomplete CSNB, due to variants in *CACNA1F*, with common features of nystagmus, foveal hypoplasia visible on OCT, and subnormal VA (144,145). OCT in 3 patients with *GRM6* variants (AR CSNB) identified selective thinning of the inner retinal layers suggesting either reduced bipolar or ganglion cell numbers or altered synaptic structure in the inner retina (146).

FA

FA is an AR disease characterized by multiple white subretinal spots (147), throughout the retina (Figure 6A). FA has been attributed to variants in *RDH5*, *RLBP1* and *RPE65* (148). *RDH5* retinopathy (also *RPE65* and *RLBP1*, albeit to a lesser extent) leads to reduced AF signal possibly because of absence of retinoid-derived fluorophores (147). The white dots in younger subjects appear as foci of increased signal on FAF imaging (Figure 6A). On OCT

imaging the associated deposits extend from Bruch's membrane to the external limiting membrane, with a focal loss of photoreceptor outer segments (147). Development of macular atrophy/cone dysfunction can be observed in a later stage of the disease (149–151).

Oguchi disease

Oguchi (*SAG, GRK1*) disease is a rare form of AR CSNB having the distinguishing feature of the Mizuo-Nakamura phenomenon: diffuse green-golden fundus discoloration in the presence of light (Figure 6B) which returns to normal after prolonged dark adaptation (141,152) Foveal retinal thickness can be normal on OCT (Figure 6B) (146). AOSLO identified that rods, but not cones, change intensity after dark adaptation, suggesting that the fundus changes are the result of changes within the rods as opposed to changes at a different retinal locus (146). Development of peripheral atrophy is observed in a later stage of the disease (153).

Chorioretinal dystrophies

Choroideremia (CHM)

CHM (*CHM*, OMIM 300390) is a rare X-linked condition characterized by degeneration of the choriocapillaris, RPE and retina (Figure 7A), with males presenting in early adulthood or late childhood with nyctalopia and constricted peripheral vision (154). The skewed X-inactivation can lead to symptomatic female carriers (Figure 7B), sharing similar imaging characteristics to affected males. FAF of the disease allows direct visualization of the choroidal vessels due to loss of the photoreceptor layers and the RPE, with a residual asymmetric central area of functioning retina.

Common OCT findings include IZ attenuation, with or without intact EZ, outer retinal tubulations, interlaminar bridges and RPE thinning (155–157). AOSLO has been employed extensively, demonstrating a normal photoreceptor mosaic in asymptomatic carriers and patchy cone loss in symptomatic carriers (155). Affected males have disrupted parafoveal mosaics, with increased cone spacing. The cone spacing is more regular near the borders of atrophy (155). The largest multimodal study to date including the use of AOSLO (156), describes a relatively intact central retina with a normal or reduced cone density at 0.5 mm eccentricity; and an abrupt loss of cones at the border of RPE atrophy, as well as hyper-reflective clumps of cones in younger patients (<30 years) and bubble-like lesions within the choroid (157). IZ drop-out precedes EZ disruption and no RPE cells were visible in areas of cone loss (156). Investigators thereby proposed that CHM is primarily an RPE disorder followed by photoreceptor degeneration; recent OCTA studies have similar conclusions. A phase II/III gene therapy trial is on-going.

Gyrate atrophy (GA)

GA (*OAT*, OMIM 613349) is a rare in-born error of metabolism with retinal manifestations of progressive chorioretinal loss, beginning as small areas of peripheral RPE and choroidal atrophy, which coalesce to larger well demarcated atrophic area, visible on FAF as area of decreased AF (Figure 7C) (158). On OCT macular oedema can be seen, as well as retinal tubulations in advanced disease (158,159).

Concluding remarks & future prospects

Advances in molecular genetic techniques have greatly simplified molecular diagnosis. Similarly, advances in retinal imaging and retinal function testing have improved knowledge of disease natural history, which is key to identifying treatment effects in clinical trials of novel therapies. The remaining challenge is to develop novel therapies that will slow degeneration or improve function. The ongoing and upcoming trials emphasise the increasing need for further detailed investigation of retinal structure, to better explore the natural history of the diseases, the reliability and repeatability of the different imaging methods and measurements, and moreover define inclusion criteria, prognostic indicators and endpoints.

Acknowledgments

Funding: Supported by grants from the National Institute for Health Research Biomedical Research Centre at Moorfields Eye Hospital NHS Foundation Trust and UCL Institute of Ophthalmology, Macular Society (UK), Fight for Sight (UK), Onassis Foundation, Leventis Foundation, The Wellcome Trust (099173/Z/12/Z), Moorfields Eye Hospital Special Trustees, Moorfields Eye Charity, Retina UK, and the Foundation Fighting Blindness (USA).

References

1. Liew G, Michaelides M, Bunce C. A comparison of the causes of blindness certifications in England and Wales in working age adults (16–64 years), 1999–2000 with 2009–2010. *BMJ Open* 2014;4:e004015.
2. Galvin O, Chi G, Brady L, et al. The Impact of Inherited Retinal Diseases in the Republic of Ireland (ROI) and the United Kingdom (UK) from a Cost-of-Illness Perspective. *Clin Ophthalmol* 2020;14:707–19. [PubMed: 32184557]
3. Smith J, Ward D, Michaelides M, et al. New and emerging technologies for the treatment of inherited retinal diseases: a horizon scanning review. *Eye (Lond)* 2015;29:1131–40. [PubMed: 26113499]
4. Rahman N, Georgiou M, Khan KN, et al. Macular dystrophies: clinical and imaging features, molecular genetics and therapeutic options. *Br J Ophthalmol* 2020;104:451–60. [PubMed: 31704701]
5. Pontikos N, Arno G, Jurkute N, et al. Genetic basis of inherited retinal disease in a molecularly characterised cohort of over 3000 families from the United Kingdom. *Ophthalmology* 2020. [Epub ahead of print].
6. Khan KN, Kasilian M, Mahroo OAR, et al. Early Patterns of Macular Degeneration in ABCA4-Associated Retinopathy. *Ophthalmology* 2018;125:735–46. [PubMed: 29310964]
7. Tanna P, Georgiou M, Strauss RW, et al. Cross-Sectional and Longitudinal Assessment of the Ellipsoid Zone in Childhood-Onset Stargardt Disease. *Transl Vis Sci Technol* 2019;8:1.
8. Fujinami K, Zernant J, Chana RK, et al. Clinical and molecular characteristics of childhood-onset Stargardt disease. *Ophthalmology* 2015;122:326–34. [PubMed: 25312043]
9. Fujinami K, Sergouniotis PI, Davidson AE, et al. Clinical and molecular analysis of Stargardt disease with preserved foveal structure and function. *Am J Ophthalmol* 2013;156:487–501.e1. [PubMed: 23953153]
10. Tanna P, Georgiou M, Aboshiha J, et al. Cross-Sectional and Longitudinal Assessment of Retinal Sensitivity in Patients With Childhood-Onset Stargardt Disease. *Transl Vis Sci Technol* 2018;7:10.
11. Gill JS, Georgiou M, Kalitzeos A, et al. Progressive cone and cone-rod dystrophies: clinical features, molecular genetics and prospects for therapy. *Br J Ophthalmol* 2019;103:711–20.
12. Strauss RW, Kong X, Ho A, et al. Progression of Stargardt Disease as Determined by Fundus Autofluorescence Over a 12-Month Period: ProgStar Report No. 11. *JAMA Ophthalmol* 2019;137:1134–45.

13. Georgiou M, Kane T, Tanna P, et al. Prospective Cohort Study of Childhood-Onset Stargardt Disease: Fundus Autofluorescence Imaging, Progression, Comparison with Adult-Onset Disease, and Disease Symmetry. *Am J Ophthalmol* 2020;211:159–75. [PubMed: 31812472]
14. Strauss RW, Munoz B, Ho A, et al. Incidence of Atrophic Lesions in Stargardt Disease in the Progression of Atrophy Secondary to Stargardt Disease (ProgStar) Study: Report No. 5. *JAMA Ophthalmol* 2017;135:687–95. [PubMed: 28542697]
15. Strauss RW, Munoz B, Ho A, et al. Progression of Stargardt Disease as Determined by Fundus Autofluorescence in the Retrospective Progression of Stargardt Disease Study (ProgStar Report No. 9). *JAMA Ophthalmol* 2017;135:1232–41. [PubMed: 29049437]
16. Chen L, Lee W, de Carvalho JRL Jr, et al. Multi-platform imaging in ABCA4-Associated Disease. *Sci Rep* 2019;9:6436. [PubMed: 31015497]
17. Klufas MA, Tsui I, Sadda SR, et al. Ultrawidefield autofluorescence in ABCA4 stargardt disease. *Retina* 2018;38:403–15. [PubMed: 28248825]
18. Cai CX, Light JG, Handa JT. Quantifying the Rate of Ellipsoid Zone Loss in Stargardt Disease. *Am J Ophthalmol* 2018;186:1–9. [PubMed: 29126757]
19. Melillo P, Testa F, Rossi S, et al. En Face Spectral-Domain Optical Coherence Tomography for the Monitoring of Lesion Area Progression in Stargardt Disease. *Invest Ophthalmol Vis Sci* 2016;57:OCT247–52.
20. Greenstein VC, Nunez J, Lee W, et al. A Comparison of En Face Optical Coherence Tomography and Fundus Autofluorescence in Stargardt Disease. *Invest Ophthalmol Vis Sci* 2017;58:5227–36. [PubMed: 29049723]
21. Ritter M, Zotter S, Schmidt WM, et al. Characterization of stargardt disease using polarization-sensitive optical coherence tomography and fundus autofluorescence imaging. *Invest Ophthalmol Vis Sci* 2013;54:6416–25. [PubMed: 23882696]
22. Ergun E, Hermann B, Wirtitsch M, et al. Assessment of central visual function in Stargardt's disease/fundus flavimaculatus with ultrahigh-resolution optical coherence tomography. *Invest Ophthalmol Vis Sci* 2005;46:310–6. [PubMed: 15623790]
23. Georgiou M, Kalitzeos A, Patterson EJ, et al. Adaptive optics imaging of inherited retinal diseases. *Br J Ophthalmol* 2018;102:1028–35. [PubMed: 29141905]
24. Strauss RW, Munoz B, Wolfson Y, et al. Assessment of estimated retinal atrophy progression in Stargardt macular dystrophy using spectral-domain optical coherence tomography. *Br J Ophthalmol* 2016;100:956–62. [PubMed: 26568636]
25. Song H, Rossi EA, Latchney L, et al. Cone and rod loss in Stargardt disease revealed by adaptive optics scanning light ophthalmoscopy. *JAMA Ophthalmol* 2015;133:1198–203. [PubMed: 26247787]
26. Song H, Rossi EA, Yang Q, et al. High-Resolution Adaptive Optics in Vivo Autofluorescence Imaging in Stargardt Disease. *JAMA Ophthalmol* 2019;137:603–9. [PubMed: 30896765]
27. Tanna P, Kasilian M, Strauss R, et al. Reliability and Repeatability of Cone Density Measurements in Patients With Stargardt Disease and RPGR-Associated Retinopathy. *Invest Ophthalmol Vis Sci* 2017;58:3608–15. [PubMed: 28738413]
28. Petrukhin K, Koisti MJ, Bakall B, et al. Identification of the gene responsible for Best macular dystrophy. *Nat Genet* 1998;19:241–7. [PubMed: 9662395]
29. JDM G. Best's disease. *Stereoscopic atlas of macular disease. Diagnosis and Treatment*. St Louis, MO: Mosby, 1997:304–11.
30. Ferrara DC, Costa RA, Tsang S, et al. Multimodal fundus imaging in Best vitelliform macular dystrophy. *Graefes Arch Clin Exp Ophthalmol* 2010;248:1377–86. [PubMed: 20414784]
31. Kumar V, Chatra K. Fibrotic pillar leads to focal choroidal excavation in Best vitelliform dystrophy. *Graefes Arch Clin Exp Ophthalmol* 2018;256:2083–7. [PubMed: 30171352]
32. Shahzad R, Siddiqui MA. Choroidal neovascularization secondary to Best vitelliform macular dystrophy detected by optical coherence tomography angiography. *J aapos* 2017;21:68–70. [PubMed: 27867022]
33. Fahim AT, Ali N, Blachley T, et al. Peripheral fundus findings in X-linked retinoschisis. *Br J Ophthalmol* 2017;101:1555–9. [PubMed: 28348004]

34. Hinds AM, Fahim A, Moore AT, et al. Bullous X linked retinoschisis: clinical features and prognosis. *Br J Ophthalmol* 2018;102:622–4. [PubMed: 28848025]
35. Berenberg TL, Van Tassel SH, Patel SN, et al. Juvenile X-Linked Retinoschisis: A Comparison of Imaging Modalities and Review of Angiographic Findings. *Retina* 2016;36:e117–9. [PubMed: 27164547]
36. Duncan JL, Ratnam K, Birch DG, et al. Abnormal cone structure in foveal schisis cavities in X-linked retinoschisis from mutations in exon 6 of the RS1 gene. *Invest Ophthalmol Vis Sci* 2011;52:9614–23. [PubMed: 22110067]
37. Mohla A, Khan K, Kasilian M, et al. OCT angiography in the management of choroidal neovascular membrane secondary to Sorsby fundus dystrophy. *BMJ Case Rep* 2016;2016:bcr2016216453.
38. Renner AB, Fiebig BS, Weber BH, et al. Phenotypic variability and long-term follow-up of patients with known and novel PRPH2/RDS gene mutations. *Am J Ophthalmol* 2009;147:518–30.e1. [PubMed: 19038374]
39. Evans K, Gregory CY, Wijesuriya SD, et al. Assessment of the phenotypic range seen in Doyme honeycomb retinal dystrophy. *Arch Ophthalmol* 1997;115:904–10. [PubMed: 9230832]
40. Michaelides M, Jenkins SA, Brantley MA Jr, et al. Maculopathy due to the R345W substitution in fibulin-3: distinct clinical features, disease variability, and extent of retinal dysfunction. *Invest Ophthalmol Vis Sci* 2006;47:3085–97. [PubMed: 16799055]
41. Souied EH, Leveziel N, Letien V, et al. Optical coherent tomography features of malattia leventinese. *Am J Ophthalmol* 2006;141:404–7. [PubMed: 16458713]
42. Gerth C, Zawadzki RJ, Werner JS, et al. Retinal microstructure in patients with EFEMP1 retinal dystrophy evaluated by Fourier domain OCT. *Eye (Lond)* 2009;23:480–3. [PubMed: 18791549]
43. Serra R, Coscas F, Messaoudi N, et al. Choroidal Neovascularization in Malattia Leventinese Diagnosed Using Optical Coherence Tomography Angiography. *Am J Ophthalmol* 2017;176:108–17. [PubMed: 28088509]
44. Guimaraes TAC, Georgiou M, Robson AG, et al. KCNV2 retinopathy: clinical features, molecular genetics and directions for future therapy. *Ophthalmic Genet* 2020;41:208–15. [PubMed: 32441199]
45. Michaelides M, Hardcastle AJ, Hunt DM, et al. Progressive cone and cone-rod dystrophies: phenotypes and underlying molecular genetic basis. *Surv Ophthalmol* 2006;51:232–58. [PubMed: 16644365]
46. Michaelides M, Wilkie SE, Jenkins S, et al. Mutation in the gene GUCA1A, encoding guanylate cyclase-activating protein 1, causes cone, cone-rod, and macular dystrophy. *Ophthalmology* 2005;112:1442–7. [PubMed: 15953638]
47. Chen X, Sheng X, Zhuang W, et al. GUCA1A mutation causes maculopathy in a five-generation family with a wide spectrum of severity. *Genet Med* 2017;19:945–54. [PubMed: 28125083]
48. Song H, Rossi EA, Stone E, et al. Phenotypic diversity in autosomal-dominant cone-rod dystrophy elucidated by adaptive optics retinal imaging. *Br J Ophthalmol* 2018;102:136–41. [PubMed: 29074494]
49. Xiao X, Guo X, Jia X, et al. A recurrent mutation in GUCY2D associated with autosomal dominant cone dystrophy in a Chinese family. *Mol Vis* 2011;17:3271–8. [PubMed: 22194653]
50. Zhao X, Ren Y, Zhang X, et al. A novel GUCY2D mutation in a Chinese family with dominant cone dystrophy. *Mol Vis* 2013;19:1039–46. [PubMed: 23734073]
51. Bouzia Z, Georgiou M, Hull S, et al. GUCY2D- Associated Leber Congenital Amaurosis: A Retrospective Natural History Study in Preparation for Trials of Novel Therapies. *Am J Ophthalmol* 2020;210:59–70. [PubMed: 31704230]
52. Small KW, Silva-Garcia R, Udar N, et al. New mutation, P575L, in the GUCY2D gene in a family with autosomal dominant progressive cone degeneration. *Arch Ophthalmol* 2008;126:397–403. [PubMed: 18332321]
53. Gregory-Evans K, Kelsell RE, Gregory-Evans CY, et al. Autosomal dominant cone-rod retinal dystrophy (CORD6) from heterozygous mutation of GUCY2D, which encodes retinal guanylate cyclase. *Ophthalmology* 2000;107:55–61. [PubMed: 10647719]

54. Tsokolas G, Almuhtaseb H, Griffiths H, et al. Long term follow-up of a family with GUCY2D dominant cone dystrophy. *Int J Ophthalmol* 2018;11:1945–50. [PubMed: 30588428]
55. Michaelides M, Holder GE, Bradshaw K, et al. Cone-rod dystrophy, intrafamilial variability, and incomplete penetrance associated with the R172W mutation in the peripherin/RDS gene. *Ophthalmology* 2005;112:1592–8. [PubMed: 16019073]
56. Duncan JL, Talcott KE, Ratnam K, et al. Cone structure in retinal degeneration associated with mutations in the peripherin/RDS gene. *Invest Ophthalmol Vis Sci* 2011;52:1557–66. [PubMed: 21071739]
57. Gocho K, Akeo K, Itoh N, et al. High-Resolution Adaptive Optics Retinal Image Analysis at Early Stage Central Areolar Choroidal Dystrophy With PRPH2 Mutation. *Ophthalmic Surg Lasers Imaging Retina* 2016;47:1115–26. [PubMed: 27977834]
58. Westeneng-van Haften SC, Boon CJF, Cremers FPM, et al. Clinical and Genetic Characteristics of Late-onset Stargardt's Disease. *Ophthalmology* 2012;119:1199–210. [PubMed: 22449572]
59. Fujinami K, Lois N, Mukherjee R, et al. A Longitudinal Study of Stargardt Disease: Quantitative Assessment of Fundus Autofluorescence, Progression, and Genotype Correlations. *Invest Ophthalmol Vis Sci* 2013;54:8181–90. [PubMed: 24265018]
60. Michaelides M, Chen LL, Brantley MA Jr, et al. ABCA4 mutations and discordant ABCA4 alleles in patients and siblings with bull's-eye maculopathy. *Br J Ophthalmol* 2007;91:1650–5. [PubMed: 18024811]
61. Chen Y, Ratnam K, Sundquist SM, et al. Cone photoreceptor abnormalities correlate with vision loss in patients with Stargardt disease. *Invest Ophthalmol Vis Sci* 2011;52:3281–92. [PubMed: 21296825]
62. Shu X, Black GC, Rice JM, et al. RPGR mutation analysis and disease: an update. *Hum Mutat* 2007;28:322–8. [PubMed: 17195164]
63. Ebenezer ND, Michaelides M, Jenkins SA, et al. Identification of novel RPGR ORF15 mutations in X-linked progressive cone-rod dystrophy (XLCORD) families. *Invest Ophthalmol Vis Sci* 2005;46:1891–8. [PubMed: 15914600]
64. Robson AG, Michaelides M, Luong VA, et al. Functional correlates of fundus autofluorescence abnormalities in patients with RPGR or RIMS1 mutations causing cone or cone rod dystrophy. *Br J Ophthalmol* 2008;92:95–102. [PubMed: 17962389]
65. Tee JLL, Kalitzeos A, Webster AR, et al. Quantitative Analysis of Hyperautofluorescent Rings to Characterize the Natural History and Progression in Rprgr-Associated Retinopathy. *Retina* 2018;38:2401–14. [PubMed: 29016458]
66. Aboshiha J, Dubis AM, Carroll J, et al. The cone dysfunction syndromes. *Br J Ophthalmol* 2016;100:115–21. [PubMed: 25770143]
67. Wissinger B, Jagle H, Kohl S, et al. Human rod monochromacy: linkage analysis and mapping of a cone photoreceptor expressed candidate gene on chromosome 2q11. *Genomics* 1998;51:325–31. [PubMed: 9721202]
68. Wissinger B, Gamer D, Jagle H, et al. CNGA3 mutations in hereditary cone photoreceptor disorders. *Am J Hum Genet* 2001;69:722–37. [PubMed: 11536077]
69. Mayer AK, Van Cauwenbergh C, Rother C, et al. CNGB3 mutation spectrum including copy number variations in 552 achromatopsia patients. *Hum Mutat* 2017;38:1579–91. [PubMed: 28795510]
70. Kohl S, Baumann B, Rosenberg T, et al. Mutations in the cone photoreceptor G-protein alpha-subunit gene GNAT2 in patients with achromatopsia. *Am J Hum Genet* 2002;71:422–5. [PubMed: 12077706]
71. Aligianis IA, Forsheh T, Johnson S, et al. Mapping of a novel locus for achromatopsia (ACHM4) to 1p and identification of a germline mutation in the alpha subunit of cone transducin (GNAT2). *J Med Genet* 2002;39:656–60. [PubMed: 12205108]
72. Kohl S, Zobor D, Chiang WC, et al. Mutations in the unfolded protein response regulator ATF6 cause the cone dysfunction disorder achromatopsia. *Nat Genet* 2015;47:757–65. [PubMed: 26029869]
73. Kohl S, Coppieters F, Meire F, et al. A nonsense mutation in PDE6H causes autosomal-recessive incomplete achromatopsia. *Am J Hum Genet* 2012;91:527–32. [PubMed: 22901948]

74. Hirji N, Aboshiha J, Georgiou M, et al. Achromatopsia: clinical features, molecular genetics, animal models and therapeutic options. *Ophthalmic Genet* 2018;39:149–57. [PubMed: 29303385]
75. Aboshiha J, Dubis AM, Cowing J, et al. A prospective longitudinal study of retinal structure and function in achromatopsia. *Invest Ophthalmol Vis Sci* 2014;55:5733–43. [PubMed: 25103266]
76. Georgiou M, Robson AG, Singh N, et al. Deep Phenotyping of PDE6C-Associated Achromatopsia. *Invest Ophthalmol Vis Sci* 2019;60:5112–23. [PubMed: 31826238]
77. Sundaram V, Wilde C, Aboshiha J, et al. Retinal structure and function in achromatopsia: implications for gene therapy. *Ophthalmology* 2014;121:234–45. [PubMed: 24148654]
78. Langlo CS, Patterson EJ, Higgins BP, et al. Residual Foveal Cone Structure in CNGB3-Associated Achromatopsia. *Invest Ophthalmol Vis Sci* 2016;57:3984–95. [PubMed: 27479814]
79. Georgiou M, Litts KM, Kalitzeos A, et al. Adaptive Optics Retinal Imaging in CNGA3-Associated Achromatopsia: Retinal Characterization, Interocular Symmetry, and Intrafamilial Variability. *Invest Ophthalmol Vis Sci* 2019;60:383–96. [PubMed: 30682209]
80. Georgiou M, Singh N, Kane T, et al. Photoreceptor Structure in GNAT2-Associated Achromatopsia. *Invest Ophthalmol Vis Sci* 2020;61:40.
81. Hirji N, Georgiou M, Kalitzeos A, et al. Longitudinal Assessment of Retinal Structure in Achromatopsia Patients With Long-Term Follow-up. *Invest Ophthalmol Vis Sci* 2018;59:5735–44. [PubMed: 30513534]
82. Mastey RR, Georgiou M, Langlo CS, et al. Characterization of Retinal Structure in ATF6-Associated Achromatopsia. *Invest Ophthalmol Vis Sci* 2019;60:2631–40. [PubMed: 31237654]
83. Genead MA, Fishman GA, Rha J, et al. Photoreceptor structure and function in patients with congenital achromatopsia. *Invest Ophthalmol Vis Sci* 2011;52:7298–308. [PubMed: 21778272]
84. Thiadens AA, Somervuo V, van den Born LI, et al. Progressive loss of cones in achromatopsia: An imaging study using spectral-domain optical coherence tomography. *Invest Ophthalmol Vis Sci* 2010;51:5952–7. [PubMed: 20574029]
85. Thomas MG, Kumar A, Kohl S, et al. High-resolution in vivo imaging in achromatopsia. *Ophthalmology* 2011;118:882–7. [PubMed: 21211844]
86. Litts KM, Georgiou M, Langlo CS, et al. Interocular symmetry of foveal cone topography in congenital achromatopsia. *Curr Eye Res* 2020. [Epub ahead of print].
87. Dubis AM, Cooper RF, Aboshiha J, et al. Genotype-dependent variability in residual cone structure in achromatopsia: toward developing metrics for assessing cone health. *Invest Ophthalmol Vis Sci* 2014;55:7303–11. [PubMed: 25277229]
88. Ueno S, Nakanishi A, Kominami T, et al. In vivo imaging of a cone mosaic in a patient with achromatopsia associated with a GNAT2 variant. *Jpn J Ophthalmol* 2017;61:92–8. [PubMed: 27718025]
89. Gardner JC, Michaelides M, Holder GE, et al. Blue cone monochromacy: causative mutations and associated phenotypes. *Mol Vis* 2009;15:876–84. [PubMed: 19421413]
90. Gardner JC, Liew G, Quan YH, et al. Three different cone opsin gene array mutational mechanisms with genotype-phenotype correlation and functional investigation of cone opsin variants. *Hum Mutat* 2014;35:1354–62. [PubMed: 25168334]
91. Carroll J, Dubra A, Gardner JC, et al. The effect of cone opsin mutations on retinal structure and the integrity of the photoreceptor mosaic. *Invest Ophthalmol Vis Sci* 2012;53:8006–15. [PubMed: 23139274]
92. Patterson EJ, Kasilian M, Kalitzeos A, et al. Assessing cone photoreceptor structure in patients with mutations in the OPN1LW/OPN1MW gene array. *Invest Ophthalmol Vis Sci* 2017;58:1257.
93. Cideciyan AV, Hufnagel RB, Carroll J, et al. Human cone visual pigment deletions spare sufficient photoreceptors to warrant gene therapy. *Hum Gene Ther* 2013;24:993–1006. [PubMed: 24067079]
94. Curcio CA, Sloan KR, Kalina RE, et al. Human photoreceptor topography. *J Comp Neurol* 1990;292:497–523. [PubMed: 2324310]
95. Curcio CA, Allen KA, Sloan KR, et al. Distribution and morphology of human cone photoreceptors stained with anti-blue opsin. *J Comp Neurol* 1991;312:610–24. [PubMed: 1722224]

96. Carroll J, Rossi EA, Porter J, et al. Deletion of the X-linked opsin gene array locus control region (LCR) results in disruption of the cone mosaic. *Vision Res* 2010;50:1989–99. [PubMed: 20638402]
97. Michaelides M, Johnson S, Bradshaw K, et al. X-linked cone dysfunction syndrome with myopia and protanopia. *Ophthalmology* 2005;112:1448–54. [PubMed: 15953640]
98. Patterson EJ, Wilk M, Langlo CS, et al. Cone Photoreceptor Structure in Patients With X-Linked Cone Dysfunction and Red-Green Color Vision Deficiency. *Invest Ophthalmol Vis Sci* 2016;57:3853–63. [PubMed: 27447086]
99. Neitz J, Wagner-Schuman M, Dubra A, et al. Cone Mosaic Disruption Caused by L/M Opsin Mutations in Bornholm Eye Disease. *Invest Ophthalmol Vis Sci* 2011;52:4896.
100. Patterson EJ, Kalitzeos A, Kasilian M, et al. Residual Cone Structure in Patients With X-Linked Cone Opsin Mutations. *Invest Ophthalmol Vis Sci* 2018;59:4238–48. [PubMed: 30128495]
101. Andersen MK, Christoffersen NL, Sander B, et al. Oligocone trichromacy: clinical and molecular genetic investigations. *Invest Ophthalmol Vis Sci* 2010;51:89–95. [PubMed: 19797231]
102. Michaelides M, Rha J, Dees EW, et al. Integrity of the cone photoreceptor mosaic in oligocone trichromacy. *Invest Ophthalmol Vis Sci* 2011;52:4757–64. [PubMed: 21436275]
103. Nishiguchi KM, Sandberg MA, Kooijman AC, et al. Defects in RGS9 or its anchor protein R9AP in patients with slow photoreceptor deactivation. *Nature* 2004;427:75–8. [PubMed: 14702087]
104. Michaelides M, Li Z, Rana NA, et al. Novel mutations and electrophysiologic findings in RGS9- and R9AP-associated retinal dysfunction (Bradyopsia). *Ophthalmology* 2010;117:120–7.e1. [PubMed: 19818506]
105. Hartong DT, Pott JW, Kooijman AC. Six patients with bradyopsia (slow vision): clinical features and course of the disease. *Ophthalmology* 2007;114:2323–31. [PubMed: 17826834]
106. Cheng JY, Luu CD, Yong VH, et al. Bradyopsia in an Asian man. *Arch Ophthalmol* 2007;125:1138–40. [PubMed: 17698770]
107. Khan AO. The clinical presentation of bradyopsia in children. *J AAPOS* 2017;21:507–9.e1. [PubMed: 29107794]
108. Strauss RW, Dubis AM, Cooper RF, et al. Retinal Architecture in RGS9- and R9AP-Associated Retinal Dysfunction (Bradyopsia). *Am J Ophthalmol* 2015;160:1269–75.e1. [PubMed: 26343007]
109. Kumaran N, Moore AT, Weleber RG, et al. Leber congenital amaurosis/early-onset severe retinal dystrophy: clinical features, molecular genetics and therapeutic interventions. *Br J Ophthalmol* 2017;101:1147–54. [PubMed: 28689169]
110. Pasadhika S, Fishman GA, Stone EM, et al. Differential macular morphology in patients with RPE65-, CEP290-, GUCY2D-, and AIPL1-related Leber congenital amaurosis. *Invest Ophthalmol Vis Sci* 2010;51:2608–14. [PubMed: 19959640]
111. Sheck L, Davies WIL, Moradi P, et al. Leber Congenital Amaurosis Associated with Mutations in CEP290, Clinical Phenotype, and Natural History in Preparation for Trials of Novel Therapies. *Ophthalmology* 2018;125:894–903. [PubMed: 29398085]
112. Kousal B, Dudakova L, Gaillyova R, et al. Phenotypic features of CRB1-associated early-onset severe retinal dystrophy and the different molecular approaches to identifying the disease-causing variants. *Graefes Arch Clin Exp Ophthalmol* 2016;254:1833–9. [PubMed: 27113771]
113. Jacobson SG, Cideciyan AV, Aleman TS, et al. Crumbs homolog 1 (CRB1) mutations result in a thick human retina with abnormal lamination. *Hum Mol Genet* 2003;12:1073–8. [PubMed: 12700176]
114. Talib M, van Schooneveld MJ, van Genderen MM, et al. Genotypic and Phenotypic Characteristics of CRB1-Associated Retinal Dystrophies: A Long-Term Follow-up Study. *Ophthalmology* 2017;124:884–95. [PubMed: 28341475]
115. Khan KN, Robson A, Mahroo OAR, et al. A clinical and molecular characterisation of CRB1-associated maculopathy. *Eur J Hum Genet* 2018;26:687–94. [PubMed: 29391521]
116. Schuster A, Janecke AR, Wilke R, et al. The phenotype of early-onset retinal degeneration in persons with RDH12 mutations. *Invest Ophthalmol Vis Sci* 2007;48:1824–31. [PubMed: 17389517]

117. Fahim AT, Bouzia Z, Branham KH, et al. Detailed clinical characterisation, unique features and natural history of autosomal recessive RDH12-associated retinal degeneration. *Br J Ophthalmol* 2019;103:1789–96. [PubMed: 30979730]
118. Scott HA, Place EM, Ferenchak K, et al. Expanding the phenotypic spectrum in RDH12-associated retinal disease. *Cold Spring Harb Mol Case Stud* 2020;6:a004754.
119. Lorenz B, Wabbels B, Wegscheider E, et al. Lack of fundus autofluorescence to 488 nanometers from childhood on in patients with early-onset severe retinal dystrophy associated with mutations in RPE65. *Ophthalmology* 2004;111:1585–94. [PubMed: 15288992]
120. Kumaran N, Georgiou M, Bainbridge JWB, et al. Retinal Structure in RPE65-Associated Retinal Dystrophy. *Invest Ophthalmol Vis Sci* 2020;61:47.
121. Jacobson SG, Aleman TS, Cideciyan AV, et al. Identifying photoreceptors in blind eyes caused by RPE65 mutations: Prerequisite for human gene therapy success. *Proc Natl Acad Sci U S A* 2005;102:6177–82. [PubMed: 15837919]
122. Falk MJ, Zhang Q, Nakamaru-Ogiso E, et al. NMNAT1 mutations cause Leber congenital amaurosis. *Nat Genet* 2012;44:1040–5. [PubMed: 22842227]
123. Kumaran N, Robson AG, Michaelides M. A novel case series of nmnat1-associated early-onset retinal dystrophy: extending the phenotypic spectrum. *Retin Cases Brief Rep* 2018. [Epub ahead of print].
124. Aboshiha J, Dubis AM, van der Spuy J, et al. Preserved outer retina in AIPL1 Leber's congenital amaurosis: implications for gene therapy. *Ophthalmology* 2015;122:862–4. [PubMed: 25596619]
125. Tee JLL, Smith AJ, Hardcastle AJ, et al. RPGR-associated retinopathy: clinical features, molecular genetics, animal models and therapeutic options. *Br J Ophthalmol* 2016;100:1022–7. [PubMed: 26843488]
126. Hartong DT, Berson EL, Dryja TP. Retinitis pigmentosa. *Lancet* 2006;368:1795–809. [PubMed: 17113430]
127. Tee JJ, Smith AJ, Hardcastle AJ, et al. RPGR-associated retinopathy: clinical features, molecular genetics, animal models and therapeutic options. *Br J Ophthalmol* 2016;100:1022–7. [PubMed: 26843488]
128. Fahim A. Retinitis pigmentosa: recent advances and future directions in diagnosis and management. *Curr Opin Pediatr* 2018;30:725–33. [PubMed: 30234647]
129. Robson AG, El-Amir A, Bailey C, et al. Pattern ERG correlates of abnormal fundus autofluorescence in patients with retinitis pigmentosa and normal visual acuity. *Invest Ophthalmol Vis Sci* 2003;44:3544–50. [PubMed: 12882805]
130. Cabral T, Sengillo JD, Duong JK, et al. Retrospective Analysis of Structural Disease Progression in Retinitis Pigmentosa Utilizing Multimodal Imaging. *Sci Rep* 2017;7:10347. [PubMed: 28871101]
131. Jayasundera T, Branham KE, Othman M, et al. RP2 phenotype and pathogenetic correlations in X-linked retinitis pigmentosa. *Arch Ophthalmol* 2010;128:915–23. [PubMed: 20625056]
132. Tee JLL, Carroll J, Webster AR, et al. Quantitative Analysis of Retinal Structure Using Spectral-Domain Optical Coherence Tomography in RPGR-Associated Retinopathy. *Am J Ophthalmol* 2017;178:18–26. [PubMed: 28322733]
133. Birch DG, Locke KG, Wen Y, et al. Spectral-domain optical coherence tomography measures of outer segment layer progression in patients with X-linked retinitis pigmentosa. *JAMA Ophthalmol* 2013;131:1143–50. [PubMed: 23828615]
134. Coussa RG, Basali D, Maeda A, et al. Sector retinitis pigmentosa: Report of ten cases and a review of the literature. *Mol Vis* 2019;25:869–89. [PubMed: 31908405]
135. Audo I, Michaelides M, Robson AG, et al. Phenotypic variation in enhanced S-cone syndrome. *Invest Ophthalmol Vis Sci* 2008;49:2082–93. [PubMed: 18436841]
136. Jacobson SG, Sumaroka A, Aleman TS, et al. Nuclear receptor NR2E3 gene mutations distort human retinal laminar architecture and cause an unusual degeneration. *Hum Mol Genet* 2004;13:1893–902. [PubMed: 15229190]
137. Yzer S, Barbazetto I, Allikmets R, et al. Expanded clinical spectrum of enhanced S-cone syndrome. *JAMA Ophthalmol* 2013;131:1324–30. [PubMed: 23989059]

138. Khan AO, Aldahmesh MA, Al-Harhi E, et al. Helicoid subretinal fibrosis associated with a novel recessive NR2E3 mutation p.S44X. *Arch Ophthalmol* 2010;128:344–8. [PubMed: 20212206]
139. Halford S, Liew G, Mackay DS, et al. Detailed phenotypic and genotypic characterization of bietti crystalline dystrophy. *Ophthalmology* 2014;121:1174–84. [PubMed: 24480711]
140. Li A, Jiao X, Munier FL, et al. Bietti crystalline corneoretinal dystrophy is caused by mutations in the novel gene CYP4V2. *Am J Hum Genet* 2004;74:817–26. [PubMed: 15042513]
141. Zeitz C, Robson AG, Audo I. Congenital stationary night blindness: an analysis and update of genotype-phenotype correlations and pathogenic mechanisms. *Prog Retin Eye Res* 2015;45:58–110. [PubMed: 25307992]
142. Zeitz C, Friedburg C, Preising MN, et al. Overview of Congenital Stationary Night Blindness with Predominantly Normal Fundus Appearance. *Klin Monbl Augenheilkd* 2018.
143. Miyake Y, Yagasaki K, Horiguchi M, et al. Congenital stationary night blindness with negative electroretinogram. A new classification. *Arch Ophthalmol* 1986;104:1013–20. [PubMed: 3488053]
144. Hove MN, Kilic-Biyik KZ, Trotter A, et al. Clinical Characteristics, Mutation Spectrum, and Prevalence of Aland Eye Disease/Incomplete Congenital Stationary Night Blindness in Denmark. *Invest Ophthalmol Vis Sci* 2016;57:6861–9. [PubMed: 28002560]
145. Kimchi A, Meiner V, Silverstein S, et al. An Ashkenazi Jewish founder mutation in CACNA1F causes retinal phenotype in both hemizygous males and heterozygous female carriers. *Ophthalmic Genet* 2019;40:443–8. [PubMed: 31651202]
146. Godara P, Cooper RF, Sergouniotis PI, et al. Assessing retinal structure in complete congenital stationary night blindness and Oguchi disease. *Am J Ophthalmol* 2012;154:987–1001.e1. [PubMed: 22959359]
147. Sergouniotis PI, Sohn EH, Li Z, et al. Phenotypic variability in RDH5 retinopathy (Fundus Albipunctatus). *Ophthalmology* 2011;118:1661–70. [PubMed: 21529959]
148. Yang G, Liu Z, Xie S, et al. Genetic and phenotypic characteristics of four Chinese families with fundus albipunctatus. *Sci Rep* 2017;7:46285. [PubMed: 28393863]
149. Miyake Y, Shiroyama N, Sugita S, et al. Fundus albipunctatus associated with cone dystrophy. *Br J Ophthalmol* 1992;76:375–9. [PubMed: 1622952]
150. Nakamura M, Hotta Y, Tanikawa A, et al. A high association with cone dystrophy in Fundus albipunctatus caused by mutations of the RDH5 gene. *Invest Ophthalmol Vis Sci* 2000;41:3925–32. [PubMed: 11053295]
151. Nakamura M, Skalet J, Miyake Y. RDH5 gene mutations and electroretinogram in fundus albipunctatus with or without macular dystrophy: RDH5 mutations and ERG in fundus albipunctatus. *Doc Ophthalmol* 2003;107:3–11. [PubMed: 12906118]
152. Dryja TP. Molecular genetics of Oguchi disease, fundus albipunctatus, and other forms of stationary night blindness: LVII Edward Jackson Memorial Lecture. *Am J Ophthalmol* 2000;130:547–63. [PubMed: 11078833]
153. Nishiguchi KM, Ikeda Y, Fujita K, et al. Phenotypic Features of Oguchi Disease and Retinitis Pigmentosa in Patients with S-Antigen Mutations: A Long-Term Follow-up Study. *Ophthalmology* 2019;126:1557–66. [PubMed: 31257036]
154. MacDonald IM, Russell L, Chan CC. Choroideremia: new findings from ocular pathology and review of recent literature. *Surv Ophthalmol* 2009;54:401–7. [PubMed: 19422966]
155. Syed R, Sundquist SM, Ratnam K, et al. High-resolution images of retinal structure in patients with choroideremia. *Invest Ophthalmol Vis Sci* 2013;54:950–61. [PubMed: 23299470]
156. Morgan JI, Han G, Klinman E, et al. High-resolution adaptive optics retinal imaging of cellular structure in choroideremia. *Invest Ophthalmol Vis Sci* 2014;55:6381–97. [PubMed: 25190651]
157. Sun LW, Johnson RD, Williams V, et al. Multimodal Imaging of Photoreceptor Structure in Choroideremia. *PLoS One* 2016;11:e0167526.
158. Sergouniotis PI, Davidson AE, Lenassi E, et al. Retinal structure, function, and molecular pathologic features in gyrate atrophy. *Ophthalmology* 2012;119:596–605. [PubMed: 22182799]
159. Goldberg NR, Greenberg JP, Laud K, et al. Outer retinal tubulation in degenerative retinal disorders. *Retina* 2013;33:1871–6. [PubMed: 23676993]

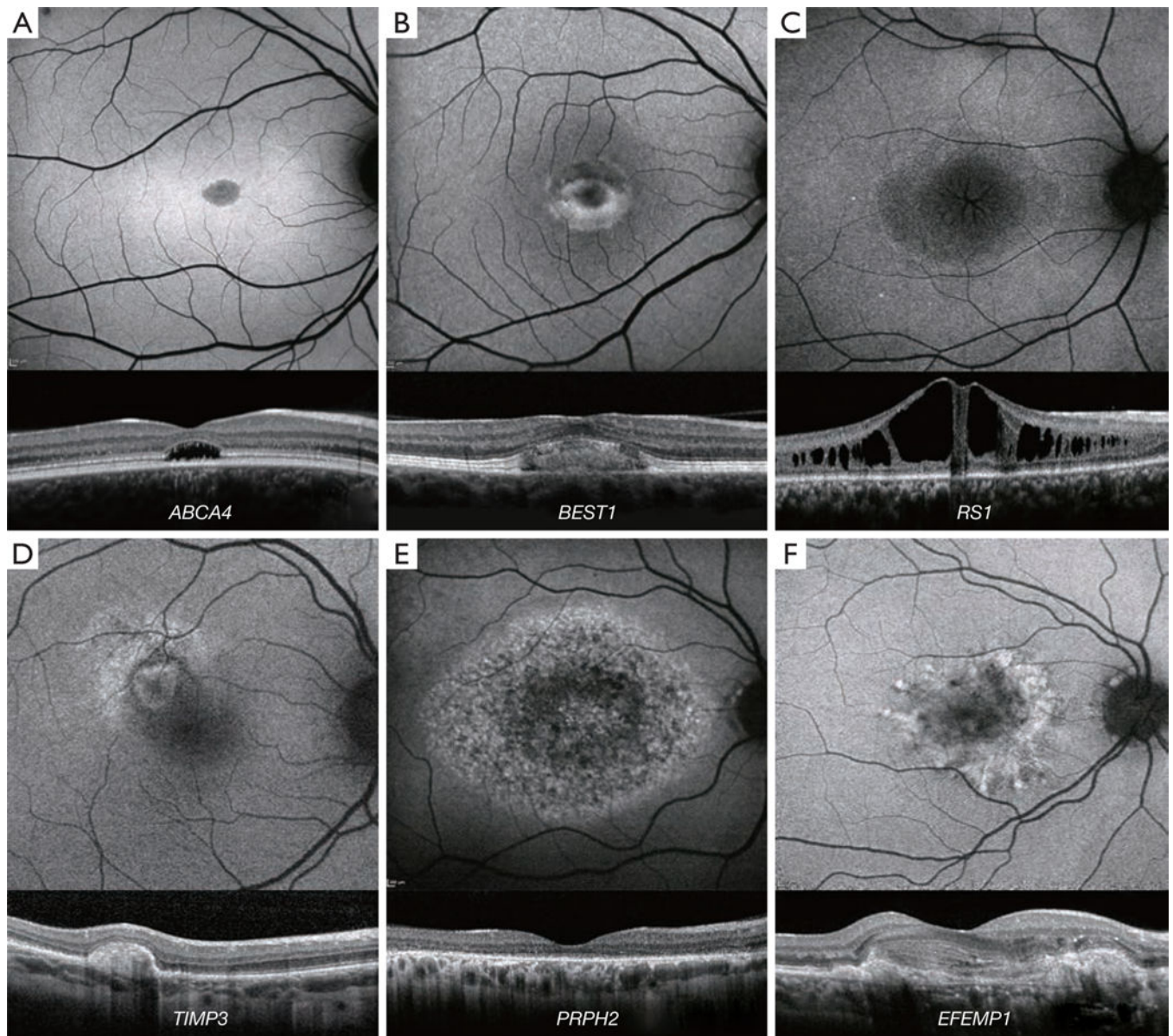


Figure 1. Retinal imaging of macular dystrophies. (A-F) Fundus autofluorescence (FAF) imaging with corresponding horizontal optical coherence tomography (OCT) scan over the region of interest. (A) Stargardt disease; isolated macular disease. (B) Best disease; vitelliform lesion, classical appearance of a single, symmetrical egg yolk-like lesion at the fovea (stage 2). (C) X-linked retinoschisis; “spoke-wheel” folds of the macula on FAF and corresponding macular schisis on OCT. (D) Sorsby fundus dystrophy; FAF imaging identifies an ill-defined increased signal in the peripheral macula, and subretinal drusenoid deposits and neovascularization on OCT, that spare the central fovea. (E) Pattern Dystrophy; hyperautofluorescent deposits on FAF, with a characteristic speckled pattern, and subretinal hyper-reflective material is seen on OCT. (F) Autosomal dominant drusen: drusen-like

radiating deposits at the macula on FAF, and hyper-reflective thickening of the RPE-Bruch membrane complex visible with OCT.

Author Manuscript

Author Manuscript

Author Manuscript

Author Manuscript

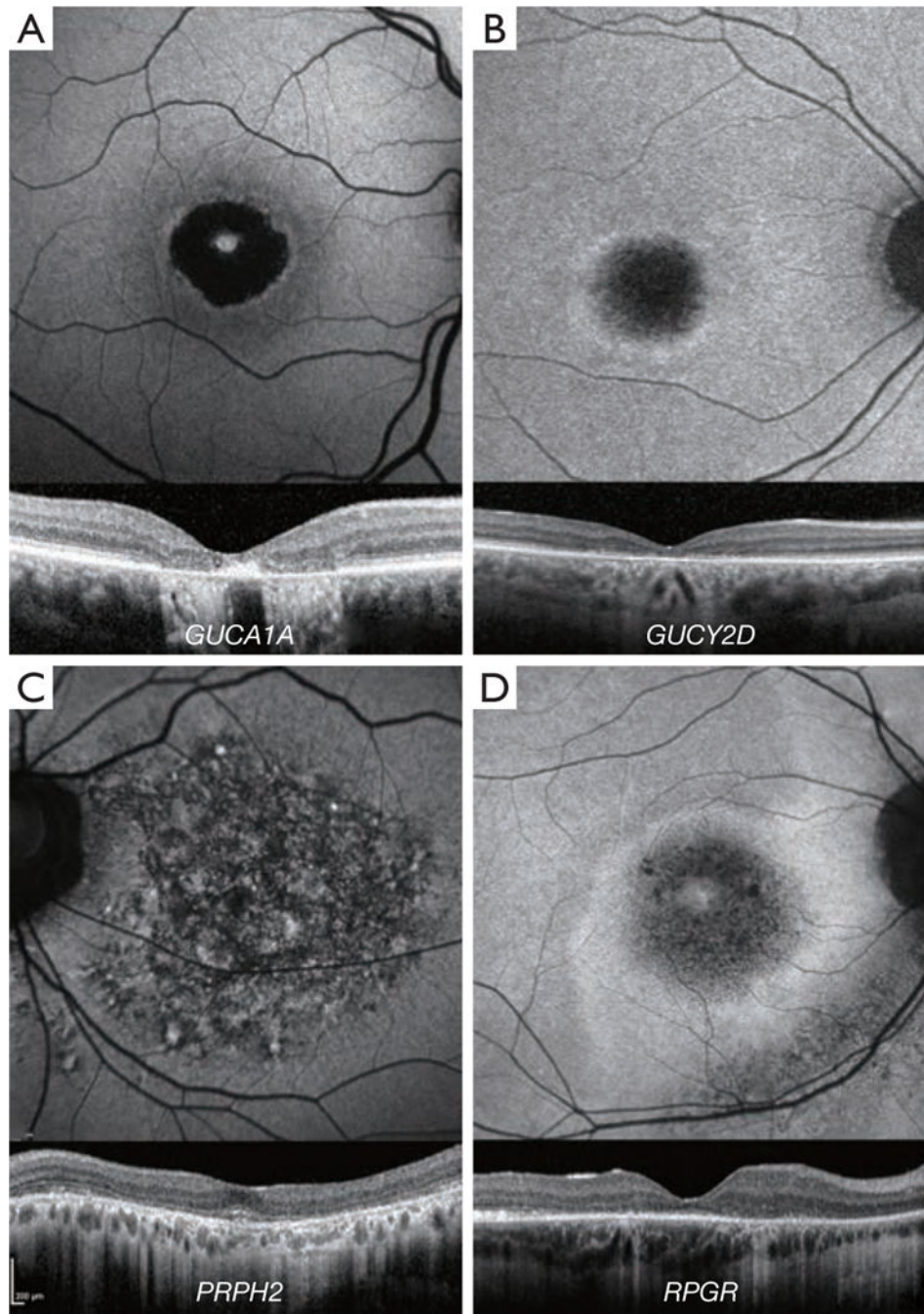


Figure 2. Retinal Imaging of Cone and Cone-Rod Dystrophies (COD/CORD). (A-C) Fundus autofluorescence (FAF) imaging with corresponding horizontal optical coherence tomography (OCT). (A) Autosomal Dominant *GUCA1A*-associated COD/CORD, with extensive macular atrophy. (B) Autosomal Dominant *GUCY2D*-associated COD/CORD, with central hypoautofluorescence and a surrounding ring of hyperautofluorescence, and foveal atrophy on OCT. (C) Autosomal Dominant *PRPH2*-associated CORD, with characteristic speckled macular appearance with FAF imaging, and loss of outer retinal

structure on OCT. (D) X-Linked *RPGR*-associated COD/CORD, with parafoveal ring of increased signal visible with FAF.

Author Manuscript

Author Manuscript

Author Manuscript

Author Manuscript

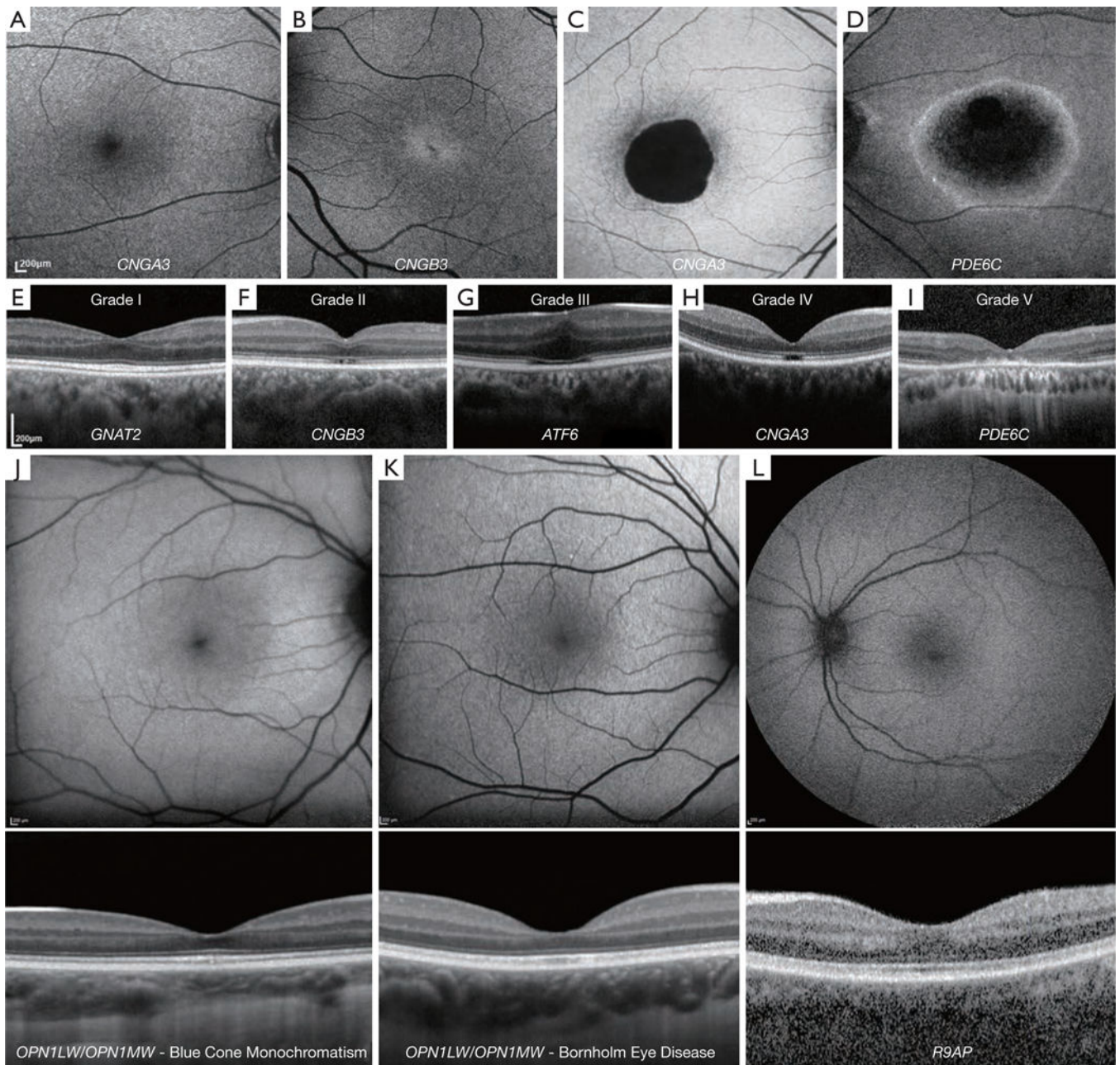


Figure 3.

Retinal Imaging of Cone Dysfunction Syndromes. Fundus autofluorescence (FAF) phenotypes in achromatopsia: (A) normal FAF appearance, (B) central increase in FAF, (C) reduced FAF signal centrally, and (D) a central area of decreased signal, with a surrounding ring of hyperautofluorescence. OCT grading in achromatopsia: (E) Grade I: continuous ellipsoid zone (EZ), (F) Grade II: EZ disruption, (G) Grade III: EZ absence, (H) Grade IV: presence of a hyporeflective zone, and (I) Grade V: outer retinal atrophy with RPE loss. Patient (F) and (G) have foveal hypoplasia, with retention of inner retinal layers at the fovea. FAF imaging with corresponding horizontal trans-foveal OCT: (J) Blue Cone

Monochromatism, (K) Bornholm Eye Disease, (L) *R9AP*-associated retinopathy ('Bradyopsia').

Author Manuscript

Author Manuscript

Author Manuscript

Author Manuscript

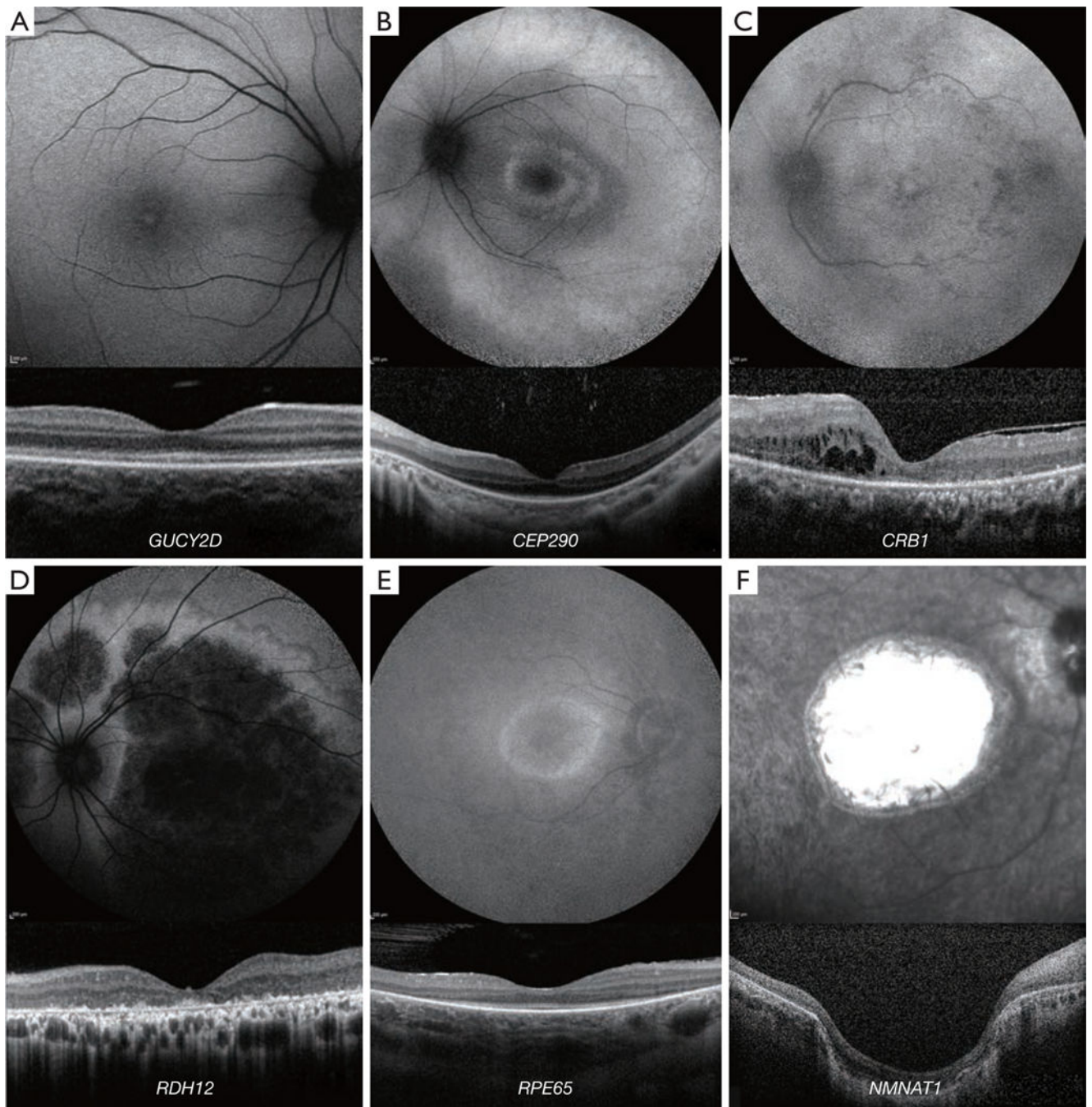


Figure 4. Retinal Imaging of Leber Congenital Amaurosis/Early-Onset Severe Retinal Dystrophy (LCA/EOSRD). (A-E) Fundus autofluorescence (FAF) imaging with corresponding horizontal trans-foveal optical coherence tomography (OCT). (A) *GUCY2D* - LCA/EOSRD; relatively preserved outer retinal structure on OCT and normal appearing FAF. (B) *CEP290* - LCA/EOSRD; preserved foveal architecture on OCT, despite profound functional loss, and FAF imaging with a perifoveal hyperautofluorescent ring. (C) *CRB1* - LCA/EOSRD; nummular pigmentation, maculopathy, relative preservation of para-arteriolar RPE on FAF,

and intraretinal cystoid spaces on OCT. (D) *RDH12* - LCA/EOSRD; FAF shows a centrally decreased signal with atrophy extending peripherally in a variegated watercolour-like fashion. OCT shows severe loss of structure and macular atrophy. (E) *RPE65* - EOSRD; reduced signal on FAF imaging and OCT showing preserved structure at the central macula. (F) *NMNAT1* - LCA; near infrared imaging and corresponding OCT scan, of a patient with severe and extensive maculopathy.

Author Manuscript

Author Manuscript

Author Manuscript

Author Manuscript

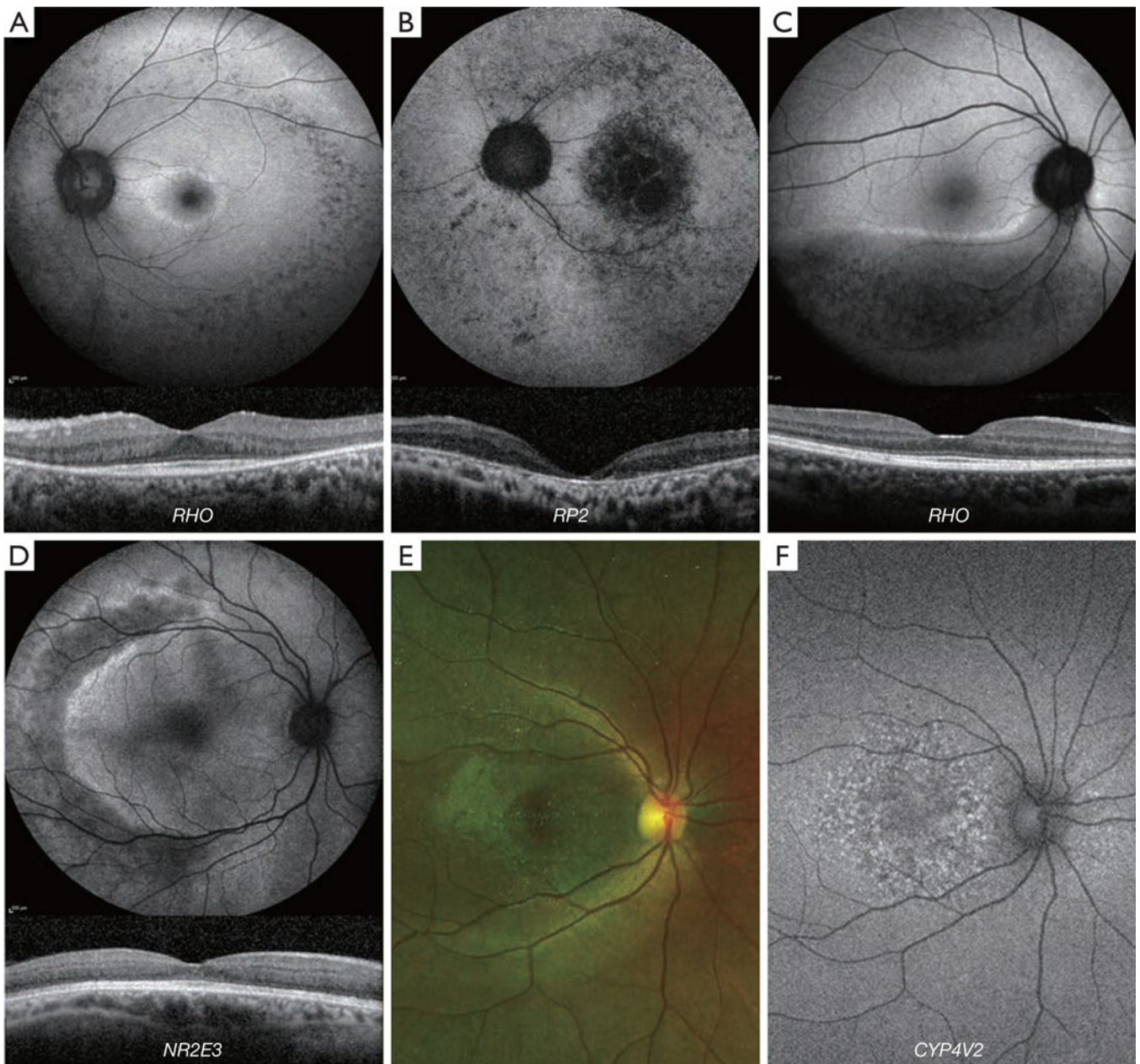


Figure 5. Retinal Imaging of Rod-Cone Dystrophies. (A) Autosomal dominant Retinitis Pigmentosa (RP) (*RHO*, Rhodopsin); patches of RPE atrophy in the mid-periphery with decreased signal on FAF and a central ring of increased signal. On OCT, there is loss of the parafoveal photoreceptors. (B) X-linked RP (*RP2*); foveal involvement with atrophy of the foveal RPE, visible on FAF, and corresponding loss of both inner and outer retina on OCT. (C) Autosomal dominant RP (*RHO*, Rhodopsin); sector pattern of retinal involvement with the inferior quadrant being affected, and a clear demarcation line of increased signal on FAF. (D) Enhanced S-cone syndrome (*NR2E3*); nummular pigment clumping at the level of the RPE, most plentiful around the temporal vascular arcades on FAF and thickened ellipsoid zone on OCT. (E) Bietti Crystalline Dystrophy (*CYP4V2*), on the left, a colour fundus

photograph showing retinal crystals, and on the right, FAF shows areas with increased and decreased signal in a speckled pattern.

Author Manuscript

Author Manuscript

Author Manuscript

Author Manuscript

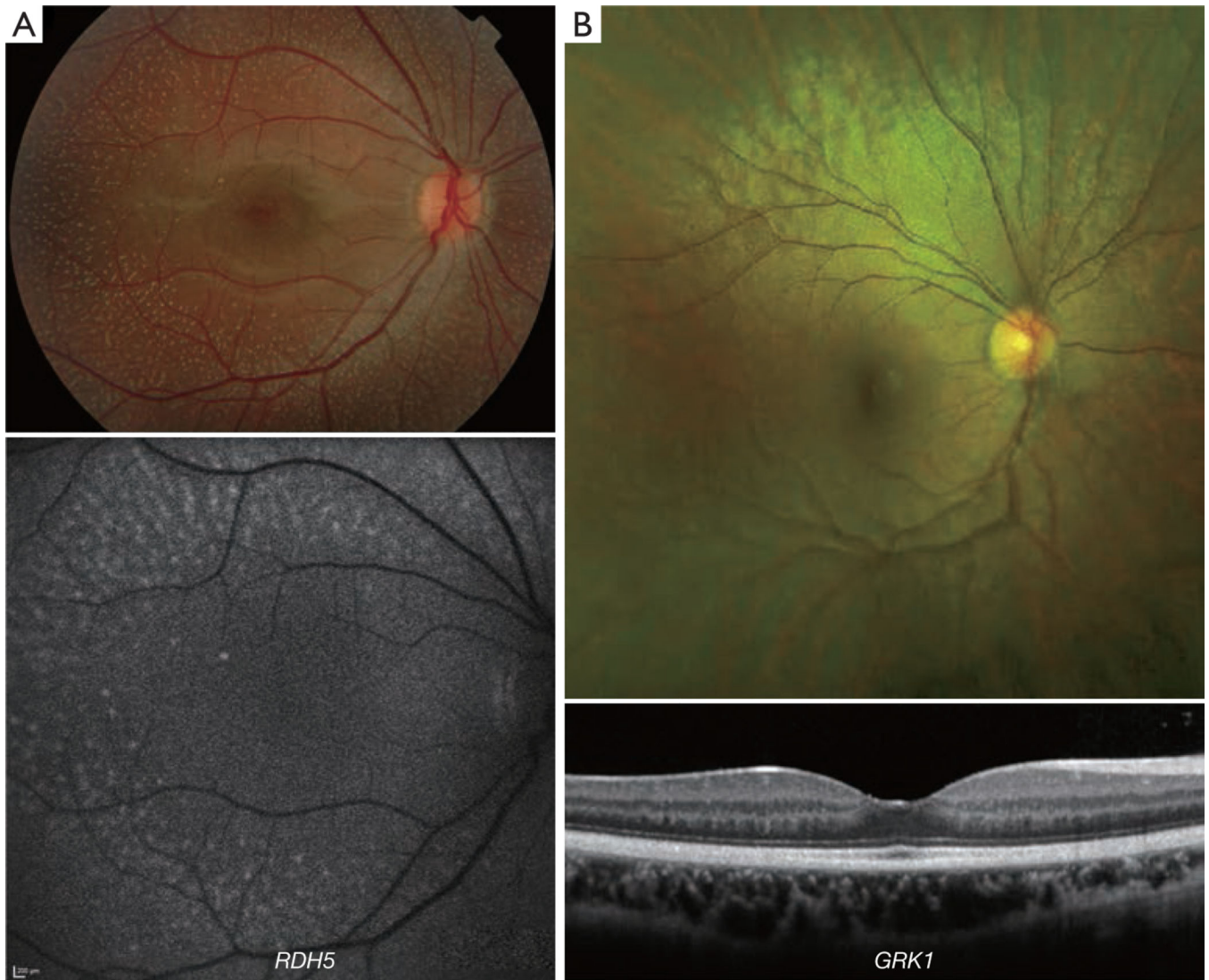


Figure 6. Retinal Imaging of Rod Dysfunction Syndromes. (A) Fundus Albipunctatus (*RDH5*); above - colour fundus photograph (CFP) with multiple white subretinal spots, throughout the retina; below - fundus autofluorescence with a diffuse reduction in signal and the white dots appearing as foci of increased signal. (B) Oguchi Disease (*GRK1*); above - CFP with diffuse green-golden fundus discolouration, and below trans-foveal optical coherence tomography with normal foveal thickness.

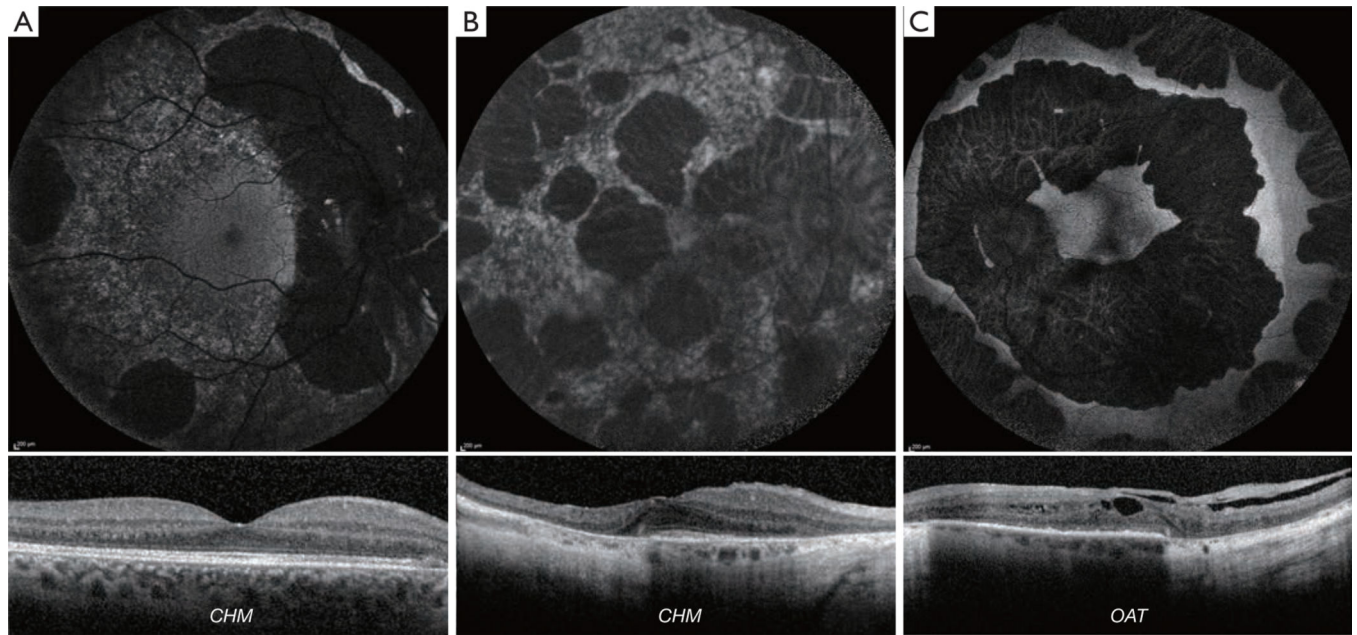


Figure 7. Retinal Imaging of Chorioretinal Dystrophies. (A-C) Fundus autofluorescence (FAF) imaging with corresponding horizontal trans-foveal optical coherence tomography (OCT). (A) Choroideremia (*CHM*) in a 35-year-old male with large areas of atrophy on FAF, not yet involving foveal center on OCT. (B) Choroideremia (*CHM*) in a severely affected 75 year old female carrier with large areas of atrophy on FAF and involving the foveal center on OCT, with a small area of spared ellipsoid zone. (C) Gyrate Atrophy (*OAT*); large well-demarcated coalesced areas of atrophy visible on FAF as decreased AF, and OCT with macular oedema and retinal tubulations.